

SCIENTIFIC REPORTS



OPEN

High-resolution 3D volumetry versus conventional measuring techniques for the assessment of experimental lymphedema in the mouse hindlimb

Received: 14 July 2016
Accepted: 16 September 2016
Published: 04 October 2016

Florian S. Frueh^{1,2,*}, Christina Körbel^{1,*}, Laura Gassert¹, Andreas Müller³, Epameinondas Gousopoulos⁴, Nicole Lindenblatt², Pietro Giovanoli², Matthias W. Laschke¹ & Michael D. Menger¹

Secondary lymphedema is a common complication of cancer treatment characterized by chronic limb swelling with interstitial inflammation. The rodent hindlimb is a widely used model for the evaluation of novel lymphedema treatments. However, the assessment of limb volume in small animals is challenging. Recently, high-resolution three-dimensional (3D) imaging modalities have been introduced for rodent limb volumetry. In the present study we evaluated the validity of microcomputed tomography (μ CT), magnetic resonance imaging (MRI) and ultrasound in comparison to conventional measuring techniques. For this purpose, acute lymphedema was induced in the mouse hindlimb by a modified popliteal lymphadenectomy. The 4-week course of this type of lymphedema was first assessed in 6 animals. In additional 12 animals, limb volumes were analyzed by μ CT, 9.4 T MRI and 30 MHz ultrasound as well as by planimetry, circumferential length and paw thickness measurements. Interobserver correlation was high for all modalities, in particular for μ CT analysis ($r = 0.975$, $p < 0.001$). Importantly, caliper-measured paw thickness correlated well with μ CT ($r = 0.861$), MRI ($r = 0.821$) and ultrasound ($r = 0.800$). Because the assessment of paw thickness represents a time- and cost-effective approach, it may be ideally suited for the quantification of rodent hindlimb lymphedema.

The lymphatic system is important for the regulation of fundamental biological processes such as immune response, intestinal lipid absorption and tissue fluid homeostasis^{1,2}. The cardinal manifestation of lymphatic dysfunction is lymphedema, a condition which is characterized by limb swelling, chronic interstitial inflammation and connective or fat tissue deposition^{3,4}. Based on the triggering cause it can be classified into primary and secondary lymphedema⁵.

Primary lymphedema has a genetic background with a dysfunctional lymphatic system, either already symptomatic after birth or later in life⁶. In contrast, acquired damage of collecting lymphatic vessels causes secondary lymphedema. In the United States, more than 5 million people suffer from cancer-related lymphedema⁷, the most common form in developed countries. Lymph node dissection and irradiation result in the formation of scar tissue, which is a key inhibitor of lymphatic regeneration⁸. In particular, breast cancer and melanoma are associated with high rates of secondary lymphedema⁹. Despite reduced surgical invasiveness, recent data indicate that 20% of female breast cancer patients undergoing axillary lymph node dissection will develop arm lymphedema¹⁰. Given the lifelong course of the disease, lymphedema has a highly relevant socio-economic burden.

Many animal models have been established for the analysis of lymphedema pathophysiology and the development of novel approaches for its treatment. However, the induction of chronic lymphedema in animals is

¹Institute for Clinical and Experimental Surgery, Saarland University, 66421 Homburg/Saar, Germany. ²Division of Plastic Surgery and Hand Surgery, University Hospital Zurich, 8091 Zurich, Switzerland. ³Clinic of Diagnostic and Interventional Radiology, Saarland University Medical Center, Homburg/Saar, Germany. ⁴Institute of Pharmaceutical Sciences, Swiss Federal Institute of Technology, ETH Zurich, Zurich, Switzerland. *These authors contributed equally to this work. Correspondence and requests for materials should be addressed to F.S.F. (email: florian.frueh@uks.eu)

challenging and requires lymphatic interruption by means of surgery and irradiation¹¹. The rodent limb is a frequently used model to study lymphatic regeneration after lymph node resection^{12,13} and emerging lymphedema treatments such as vascularized lymph node transfer^{14–18} or stem cell transplantation^{19,20}. For this purpose, the valid assessment of limb volume is a major prerequisite.

Recently, high-resolution three-dimensional (3D) imaging techniques such as magnetic resonance imaging (MRI) or microcomputed tomography (μ CT) have been introduced for rodent limb volumetry^{21,22}. However, the validity and reliability of these complex 3D techniques for limb volume assessment compared to conventional measuring techniques have not been systematically evaluated so far. Therefore, in the present study we assessed the hindlimb volumes in an acute lymphedema mouse model by means of μ CT, 9.4 T MRI and high-resolution 30 MHz ultrasound (hrUS) as well as planimetry, circumferential length and paw thickness measurements. Subsequently, we calculated interobserver variability and performed a correlation analysis for the comparison of the different techniques.

Results

Acute hindlimb lymphedema model. Acute lymphedema was induced in C57BL/6 mice by means of popliteal lymphadenectomy, circular skin incision and cautery (Fig. 1a–c). In pilot experiments, we first assessed the course of this type of acute lymphedema during 28 days. Limb swelling peaked 1 to 3 days after surgery (maximal ratio operated/non-operated leg: 1.7) and rapidly decreased throughout the following observation period (Fig. 1d–f). Noteworthy, there was still significant paw swelling after 28 days (ratio: 1.1, $p < 0.05$) (Fig. 1g). Based on these results the evaluation of different volumetric techniques was performed in groups of 3 animals between day 3 and 10 after surgery, which guaranteed a well-distributed data set for correlation analyses (Fig. 1g). Additional qualitative histological and immunohistochemical analyses revealed markedly increased paw swelling and dilated lymphatic vessels on day 3, reflecting acute lymph stasis (Fig. 1h,j). In contrast, 10 days after surgery, paw volume had decreased and lymphatic vessels exhibited normal configuration (Fig. 1i,k).

3D hindlimb volumetry. The volumes of operated and contralateral non-operated hindlimbs were assessed by means of μ CT, 9.4 T MRI and hrUS (Fig. 2a–l). The analysis included the determination of the overall volume (in mm^3) of each hindlimb. For this purpose, boundaries were manually outlined in parallel slices separated by 1 mm step size in the 3D modality images and volumes were calculated by integrating the outlined areas. Volumes were assessed with the gluteal skinfold as a landmark (Fig. 2e), because circumferential hindlimb boundaries could be outlined up to this point.

All 3D techniques resulted in high-resolution hindlimb images. In addition, due to high soft-tissue contrast, MRI and hrUS allowed visualization of edematous and thickened dermal tissue in operated hindlimbs (Fig. 2c,e,i,k). Volume assessment with hrUS was complicated by dorsal acoustic attenuation in axial images, which was overcome by extrapolation when measuring limb circumference (Fig. 2k,l). Examination times for the different 3D techniques are summarized in Table 1.

Using the gluteal skinfold as a landmark, the linear correlation between volume measurements of two observers was high for all 3D techniques (Fig. 3a,c,e). μ CT 3D volumetry showed the highest correlation with $r = 0.975$ (Fig. 3a,b). In contrast, MRI and hrUS showed a higher measurement variability between observers as illustrated by additional Bland-Altman analyses (Fig. 3d,f). Moreover, there was an insufficient correlation among 3D volumetric modalities (Fig. 4a–f). To overcome this inaccuracy, we developed a more standardized method to calculate hindlimb volumes in 3D modalities. For this purpose, the distal tibio-fibular (TF) joint was defined as a new landmark and the limb volume distal to the joint was calculated (Fig. 5). Volumes calculated using the distal TF-joint landmark correlated well among the 3D techniques (Fig. 4g–l).

The measurement of limb circumference has been frequently used to monitor experimental lymphedema in rodents. However, measuring with a string is prone to inaccuracy due to the small limb and the risk of compression. To prevent methodological inaccuracies of this conventional technique, we evaluated limb circumferences in axial T2-weighted MR images at the distal TF joint (Fig. S1a,b). This approach also allowed an accurate comparison of MRI-based limb circumferences with 3D volumes. The correlation between the two modalities was acceptable ($r = 0.796$; Fig. 6a). However, the calculation of hindlimb ratios (operated divided by non-operated leg) showed that circumferential measuring was less sensitive for the detection of lymphedema than 3D volumetry (Fig. 6b,c).

Conventional measuring techniques. The volumes of operated and contralateral non-operated hindlimbs were additionally assessed by means of planimetry, circumferential length and paw thickness measurements. For planimetric analyses, photographs of the operated and non-operated limbs were taken under a stereomicroscope and recorded on DVD. The images were analyzed by means of the software package ImageJ²³. For this purpose, we measured the limb area in a standardized template (Fig. S1c,d). Paw thickness was measured with an electronic caliper. To standardize measurements, they were performed in a transverse technique between the first and second proximal pad of the paw for all time points (Fig. S1e).

We found high interobserver correlations of all conventional measuring techniques (Fig. 3g,i,k). Caliper measurements revealed fewer outliers than the other approaches. Importantly, paw thickness correlated well with 3D volumes measured by μ CT, MRI or hrUS (Fig. 7a–f). Surprisingly, there was no correlation with two-dimensional planimetry (Fig. 7g,h) and only moderate correlation with circumferential length measurement (Fig. 7i,j). Additionally, the assessment of paw thickness resulted in higher leg ratios than the other techniques (Fig. 7b,d,f,h,j).

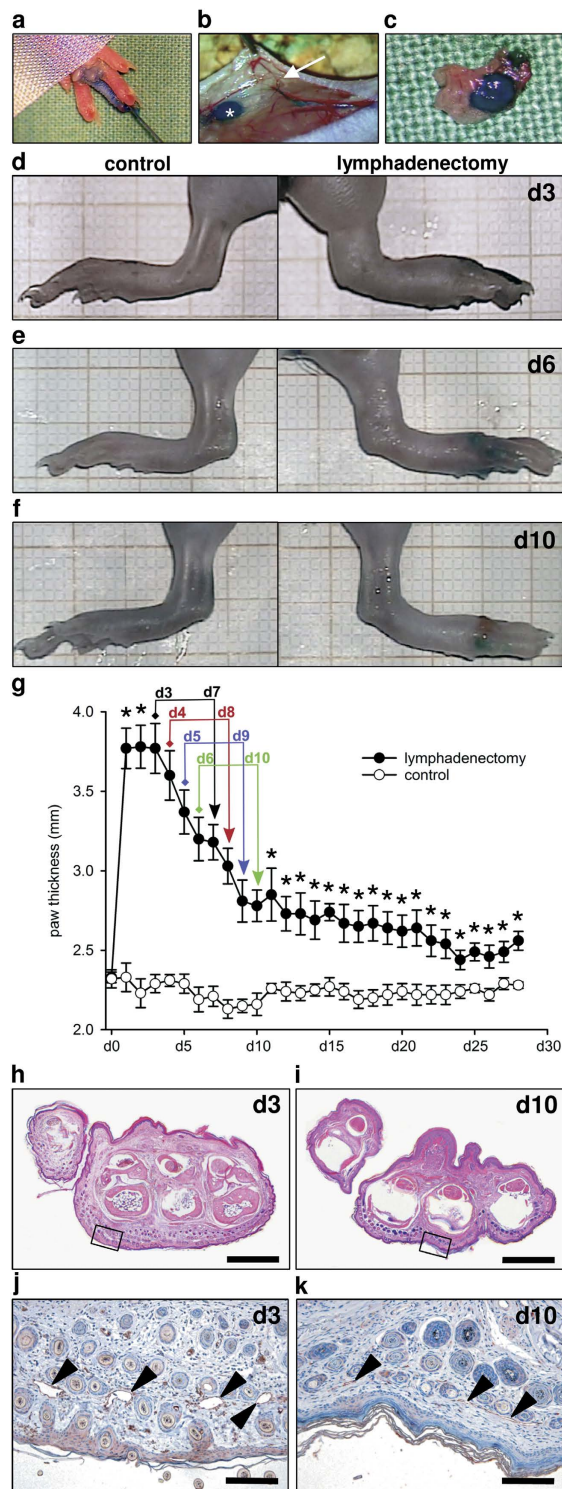


Figure 1. Animal model. (a–c) After methylene blue injection (a) the popliteal lymph node was visualized (b, asterisk). The afferent lymphatic vessels ran parallel to the iscial vein and were ligated (b, arrow). Subsequently, the popliteal fat pad including lymph nodes and efferent lymphatic vessels was resected (c). (d–f) Stereomicroscopic images illustrating paw edema with regression between day 3 (d) and day 10 (f). (g) Acute lymphedema in the mouse hindlimb over 28 days. Four experimental groups ($n = 3$ per group) were measured twice during the phase of postsurgical swelling (colored arrows) using different volumetric techniques. At the end of the experiment, there was still significant paw swelling ($n = 6$; mean \pm SEM; $*p < 0.05$). (h,i) HE-stained paw cross-sections with increased dermal thickness 3 days (h) after lymph node dissection. Ten days after surgery (i), the paw volume had markedly decreased. Scales = 1 mm. (j,k) Inserts of (h,i). Dermal lymphatic vessels were dilated on day 3 (j, arrowheads), but exhibited normal configuration on day 10 (k, arrowheads) as shown by means of immunohistochemical staining with LYVE-1. Scales = 140 μ m.

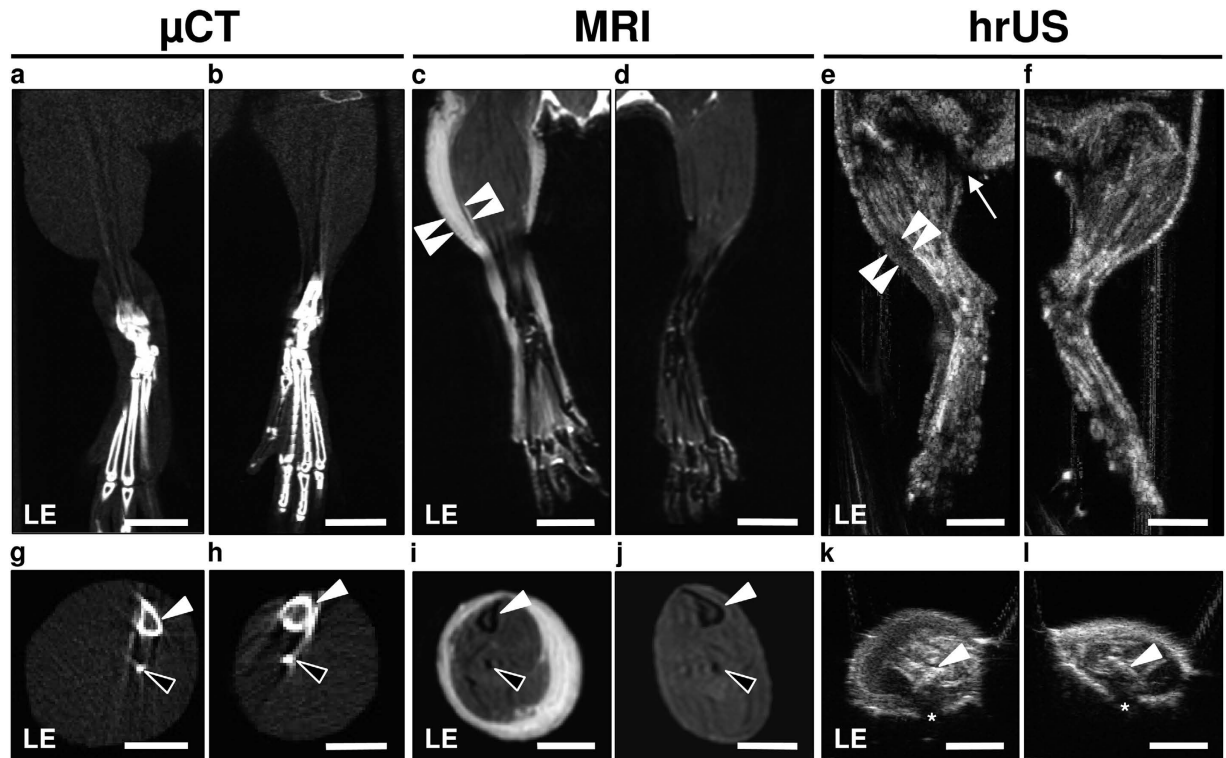


Figure 2. μ CT, MRI and hrUS for hindlimb volumetry. (a–l) Coronal (a–f) and axial (g–l) hindlimb images of μ CT (a,b,g,h), MRI (c,d,i,j) and hrUS (e,f,k,l) 3 days after popliteal lymphadenectomy. In T2-weighted MR images, the thickened and edematous tissue was characterized by epifascial hyperintensity (c, arrowheads). In contrast, 30 MHz hrUS objectified lymphedema as a hypoechoic layer (e, arrowheads). (e) Arrow = gluteal fold, which was used as a landmark for volume calculation. In axial images, tibia (g–l, white arrowhead) and fibula (g–j, black arrowheads) can be reliably identified. Note the dorsal acoustic attenuation in hrUS (k,l, asterisk). LE = lymphedema; scales (a–f) = 4.5 mm; (g–l) = 3 mm.

Modality	Costs	Examination time (min \pm SD)	Anesthesia required?	Lymphatic imaging possible?
μ CT	+++	14.6 \pm 2.2	yes	yes
MRI	+++	34.9 \pm 2.8	yes	yes
hrUS	+++	4.9 \pm 0.9	yes	no (yes)
Planimetry	++	1.0 \pm 0.3	yes	no
Circumference	+	not assessed	no	no
Caliper	+	1.2 \pm 0.2	no	no

Table 1. Features of different techniques for rodent hindlimb volumetry. 3D techniques are associated with high costs, longer examination times (i.e. time span from anesthetic induction to end of imaging) and always require anesthesia. They bear the advantage of additional lymphatic imaging using lymph-affine contrast agents. In contrast, conventional techniques are time- and cost-efficient methods to assess surrogate parameters for rodent hindlimb volumes. For maximal accuracy, hindlimb planimetry should be performed under anesthesia as well.

Discussion

The high prevalence of cancer-related lymphedema indicates urgent needs for novel treatment strategies. Microsurgical interventions to treat lymphedema include the transplantation of lymphatic vessels²⁴, lymphatico-venular anastomosis²⁵ or vascularized lymph node transfer²⁶. These approaches do not reverse the underlying pathophysiology and may only provide stabilization or delay in the development of end-stage sequelae as disfigurement and loss of function⁵.

Robust animal models, such as the rodent hindlimb, are indispensable for the establishment of novel treatments. However, beside translational issues, the lack of knowledge about the quality of volumetric modalities is a major concern in experimental lymphology¹¹. Therefore, in the present study we assessed in detail the performance of different volumetric techniques for the mouse hindlimb.

Surgery in combination with irradiation is commonly applied for the induction of chronic lymphedema in animals^{7,22}. Nonetheless, approaches inducing acute lymphatic damage without irradiation have been used for the study of vascularized lymph node transfer and growth factor treatment^{27,28}. In addition, Mendez *et al.*¹³

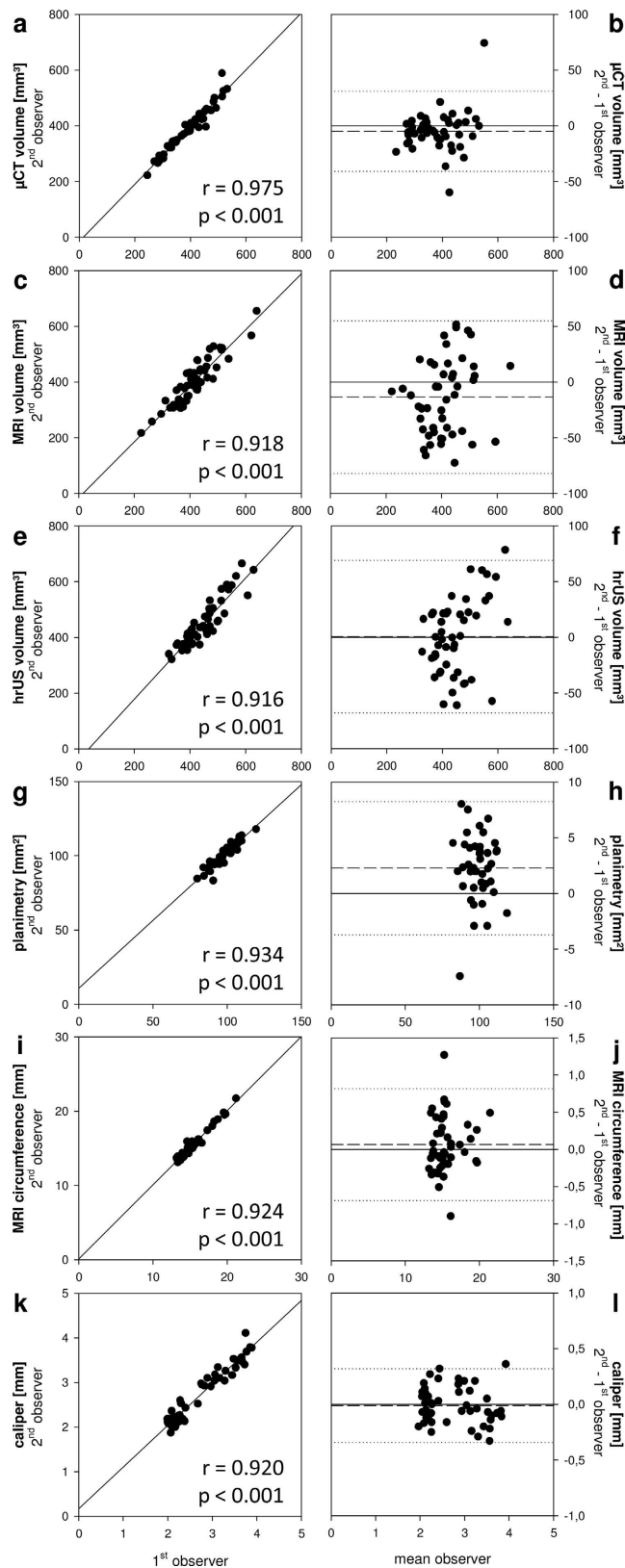


Figure 3. Interobserver variability of hindlimb volumetry modalities. (a–l) μ CT showed the highest correlation between two observers (a) and a low measurement variability (b) compared to other modalities as assessed by linear correlation (a,c,e,g,i,k) and Bland-Altman analyses (b,d,f,h,j,l). Despite low interobserver variability, MRI, hrUS, planimetry and MRI-measured circumference were associated with higher measurement variations (c–j). Dashed line = mean difference between observers; dotted line = double standard deviation. $n = 48$ for μ CT, MRI, hrUS, MRI circumference and caliper; $n = 42$ for planimetry.

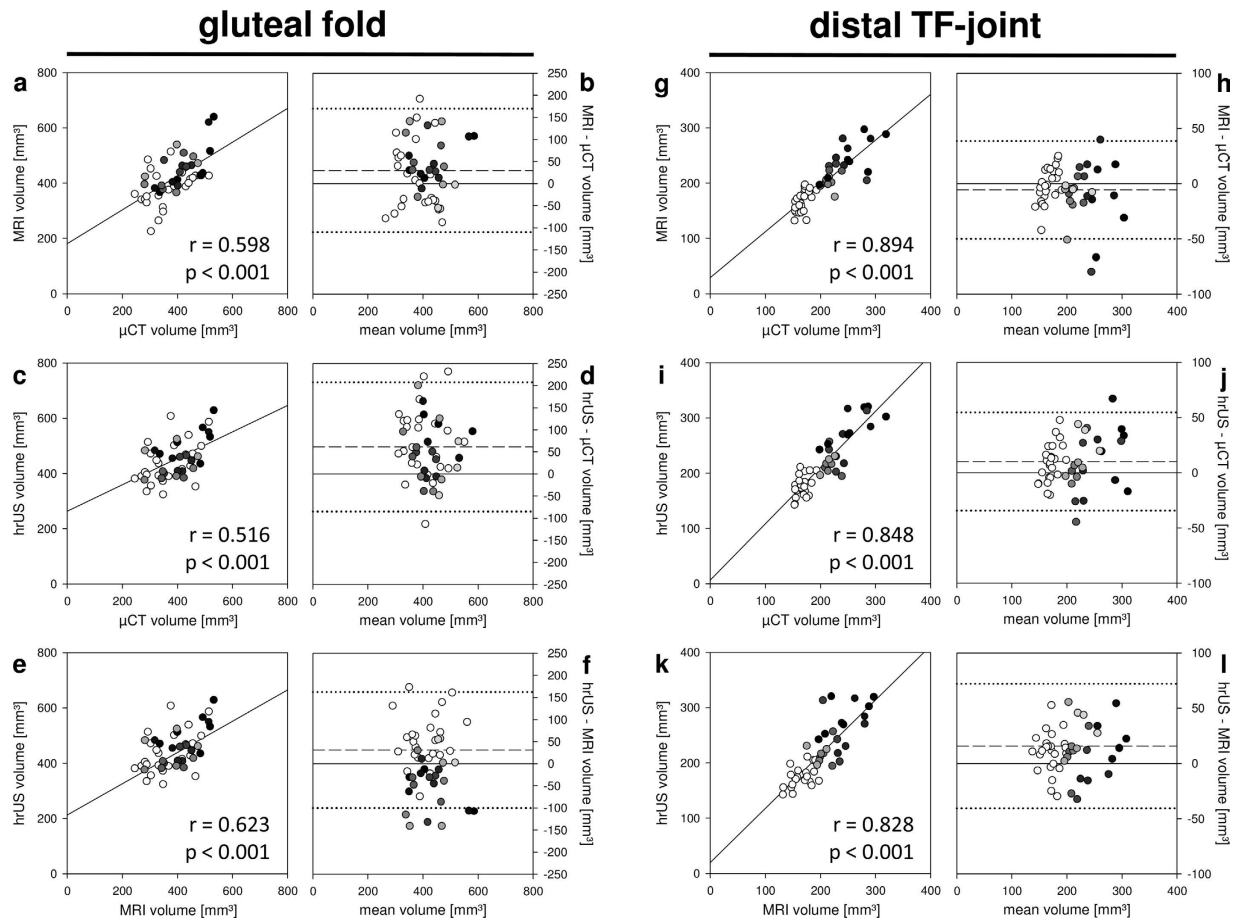


Figure 4. Correlation between different 3D volumetry modalities. (a–f) Linear correlations (a,c,e) and Bland-Altman plots (b,d,f) of 3D volumetry using the gluteal fold as landmark. Hindlimb volumes are illustrated in grey scale with non-operated controls (white circles) and operated limbs (day 3–10: black to bright grey circles). The volumes calculated with the gluteal fold landmark correlated poorly among the 3D modalities and led to a random distribution of the volumes without the expected grouping into control and operated hindlimb volumes. (g–l) After standardized measuring with the distal TF-joint landmark, 3D volumetry exhibited good correlations (g,i,k). However, the higher the hindlimb volumes, the higher the measurement variability was as shown in Bland-Altman analyses (h,j,l; black circles). Dashed line = mean difference between volume measurements; dotted line = double standard deviation; $n = 48$.

demonstrated in an acute lymphedema model of the rat forelimb that removal of axillary lymph nodes induces a chronic and latent lymphatic insufficiency. Herein, we used such a modified acute lymphedema model for the analysis of limb volumetry. The combination of radical popliteal lymphadenectomy, circular skin incision and cautery led to limb swelling which persisted up to 28 days. The rapid decrease of postsurgical hindlimb swelling was particularly useful for correlation analyses of different volumetry techniques due to a well-distributed data set.

Recently, 3D imaging modalities have been applied for limb volumetry in humans²⁹ and rodents^{21,22} with lymphedema. Little is known about their validity in comparison to conventional methods such as the assessment of circumferential length or paw thickness. Therefore, we analyzed μ CT-, MRI- and hrUS-volumetry in the mouse hindlimb. All modalities were characterized by a high interobserver correlation. We further found that high correlations between the different 3D techniques crucially depend on standardized landmarks for volume calculation. The assessment of hindlimb volumes using the gluteal fold as a landmark was inaccurate, probably due to variable positioning of the animals. In contrast, volume calculations using a more reproducible landmark, i.e. the distal TF-joint, yielded high correlation coefficients. These novel findings suggest that it may be reasonable to limit experimental 3D limb volumetry to distal parts of the extremity, as more proximal areas are hardly assessable without positioning-dependent measurement errors.

In contrast to conventional techniques, 3D volumetry modalities allow the visualization of histopathological lymphedema hallmarks such as soft tissue fibrosis and fat deposition. Moreover, they enable dynamic imaging of the lymphatic system. However, in preclinical research with small rodents, intralymphatic application of contrast agents is nearly impossible³⁰. In close analogy to human procedures, indirect MR lymphangiography with intradermal contrast application has been employed for dynamic imaging of the lymphatic system in mice^{31–33}. CT-based lymphangiography similarly depends on the development of lymph-affine contrast agents

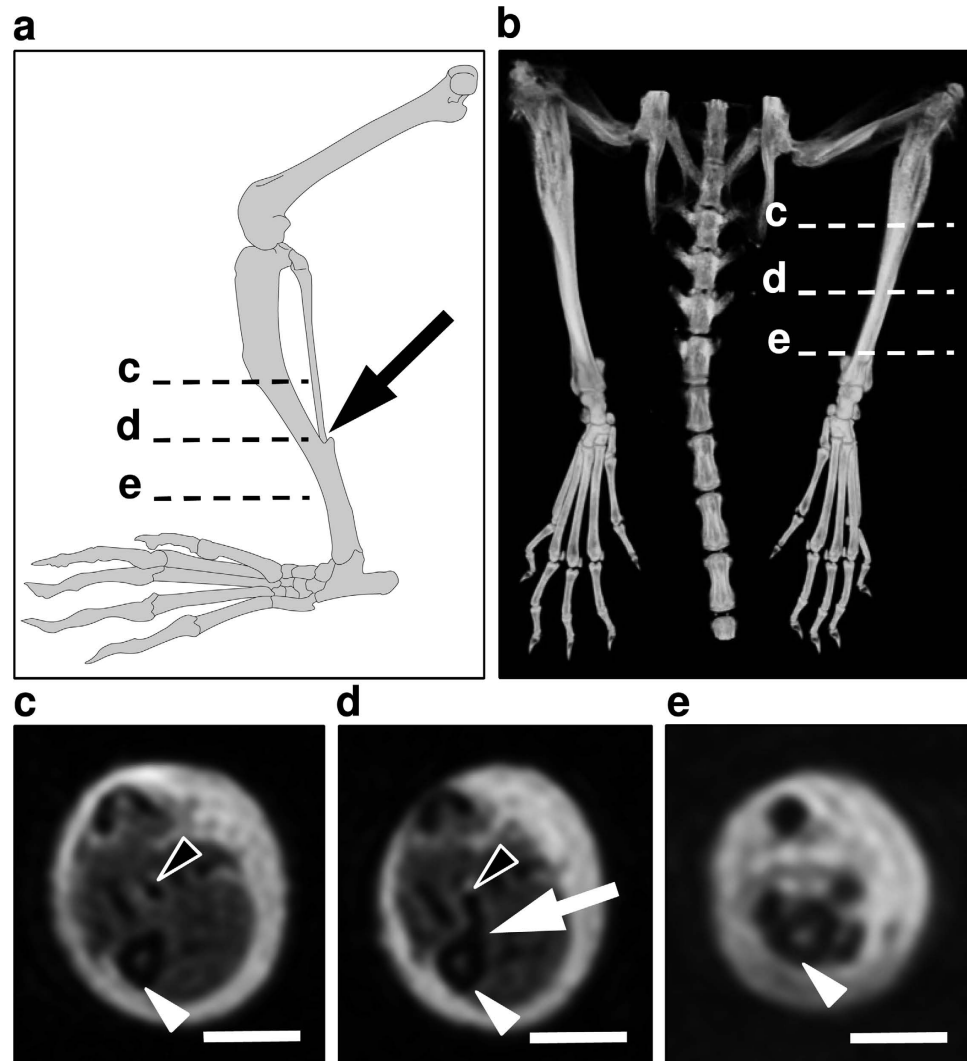


Figure 5. The distal TF-joint as landmark for standardized 3D limb volumetry. (a–e) The distal TF-joint was located in the distal third of the mouse hindlimb, as shown in an illustration (a) and 3D reconstruction of the hindlimb skeleton (b). It could be reliably localized in axial images of 3D modalities (c,d,e). Proximal to the TF-joint (c), both tibia (white arrowhead) and fibula (black arrowhead) were detectable. More distally, the two bones articulated (d, arrow). The level of the TF-joint was used for MRI-based calculations of limb circumference. (a) was drawn by Carol De Simio (University Hospital Zurich).

and promising advances have been made in the field³⁴. While μ CT and MRI are more established, photo-acoustic detection of lymphatic vessels is still in its infancy³⁵. Because most conventional contrast agents are not specifically absorbed by the lymphatic system and, thus, are not suitable for small animal lymphangiography, a broad preclinical use of MRI and μ CT for this purpose is still restricted to expensive or not commercially available products.

Many researches use conventional techniques to estimate the rodent hindlimb volume when reporting outcomes of experimental lymphedema treatment. Common parameters are the assessment of water displacement³⁶, circumferential length^{37–39} or paw thickness^{7,19}. Importantly, while well established in human lymphology⁴⁰, water displacement has been shown to yield inaccurate measurements in the mouse-tail model⁴¹. Measuring hindlimb volumes with water displacement is even more challenging due to the small and short extremities and difficult standardization. Therefore, unless plethysmometers are available^{36,42}, water displacement may be inaccurate for the assessment of rodent limb volumes. Accordingly, we did not perform water displacement in this study.

The caliper represents an inexpensive and simple tool for the assessment of rodent paw thickness. It has been used as a surrogate parameter for hindlimb volume in experimental lymphedema research^{7,19}, but its eligibility for this purpose has not been specifically analyzed. Planimetry as well as the measurement of circumferential length and paw thickness showed high interobserver correlations. Moreover, caliper-measured paw thickness was characterized by the smallest measurement variation even though it revealed the highest values for limb swelling as assessed by means of leg ratio. The correlation of the caliper measurements with all 3D volumetry modalities was high ($r = >0.8$) and Bland-Altman analyses revealed that caliper-measured leg ratios were slightly

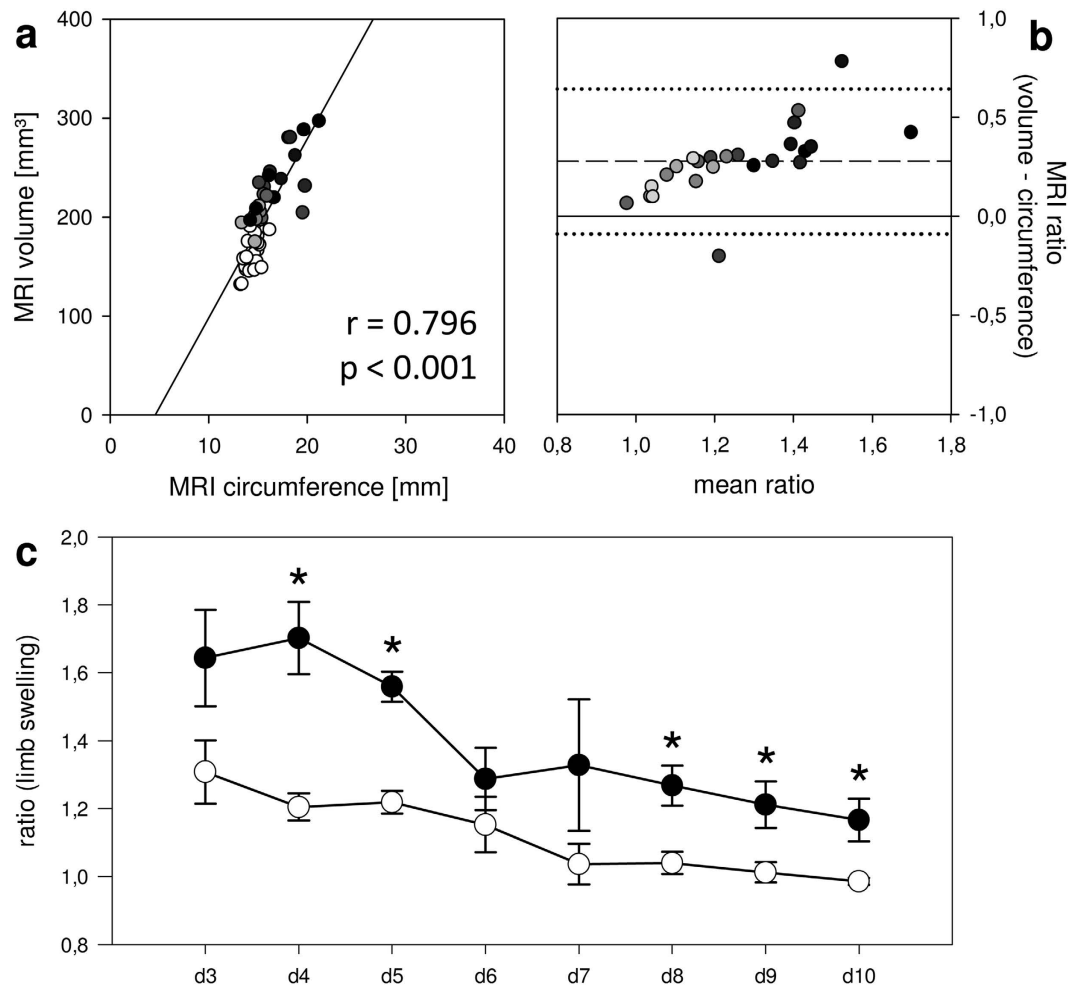


Figure 6. 3D volume and circumference measurements with MRI. (a–c) The two types of measurement correlated (a) but 3D volumetry revealed markedly higher limb ratios, as depicted by Bland-Altman analysis (b). Dashed line = mean difference between ratios; dotted line = double standard deviation; $n = 48$; day 3–10 = black to bright grey circles; non-operated control limbs = white circles. (c) Limb ratios based on 3D volumes were consistently higher throughout the course of the study (3D volume: black circles; circumference: white circles; $n = 3$ for each time point; mean \pm SEM; * $p < 0.05$).

higher than those of μ CT, MRI and hrUS. Interestingly, planimetry and circumferential length poorly correlated with paw thickness. The question, whether the caliper overestimates the ratio, i.e. the severity of lymphedema, or whether other modalities tend to underestimate the volume deserves special attention. In fact, gravitational forces influence lymphedema in humans⁴³, a phenomenon that could also aggravate rodent paw swelling. Therefore, the caliper may be especially sensitive for the assessment of rodent limb lymphedema. Furthermore, paw thickness is already a well-established parameter in experimental research of inflammatory arthritis^{44,45}.

Taken together, this study demonstrates that the calculation of hindlimb volumes in mice can be achieved in different ways. 3D techniques such as μ CT, MRI and hrUS are expensive, time-consuming and must be strictly standardized for valid and reliable measurements. In contrast, caliper-measured paw thickness may be the most suitable method to assess the course of rodent lymphedema. It represents an inexpensive, technically feasible, fast and reproducible method with a high sensitivity to detect changes of paw volume.

Methods

Animals. For the establishment of the acute lymphedema model, we used male C57BL/6 mice (Institute for Clinical & Experimental Surgery, Saarland University, Homburg/Saar, Germany) with a body weight of 28–31 g ($n = 6$). For the volumetric study, male C57BL/6 mice with a body weight of 25–27 g ($n = 12$) were used. The animals were housed one per cage with a 12-h day/night cycle and were fed ad libitum with water and standard pellet food (Atromin, Lage, Germany). The local governmental animal care committee (Landesamt für Verbraucherschutz, Saarbrücken, Germany) approved all experiments. They were conducted in accordance with the European legislation on the protection of animals (Directive 2010/63/EU) and the NIH guidelines on the care and use of laboratory animals (NIH publication #85-23 Rev. 1985).

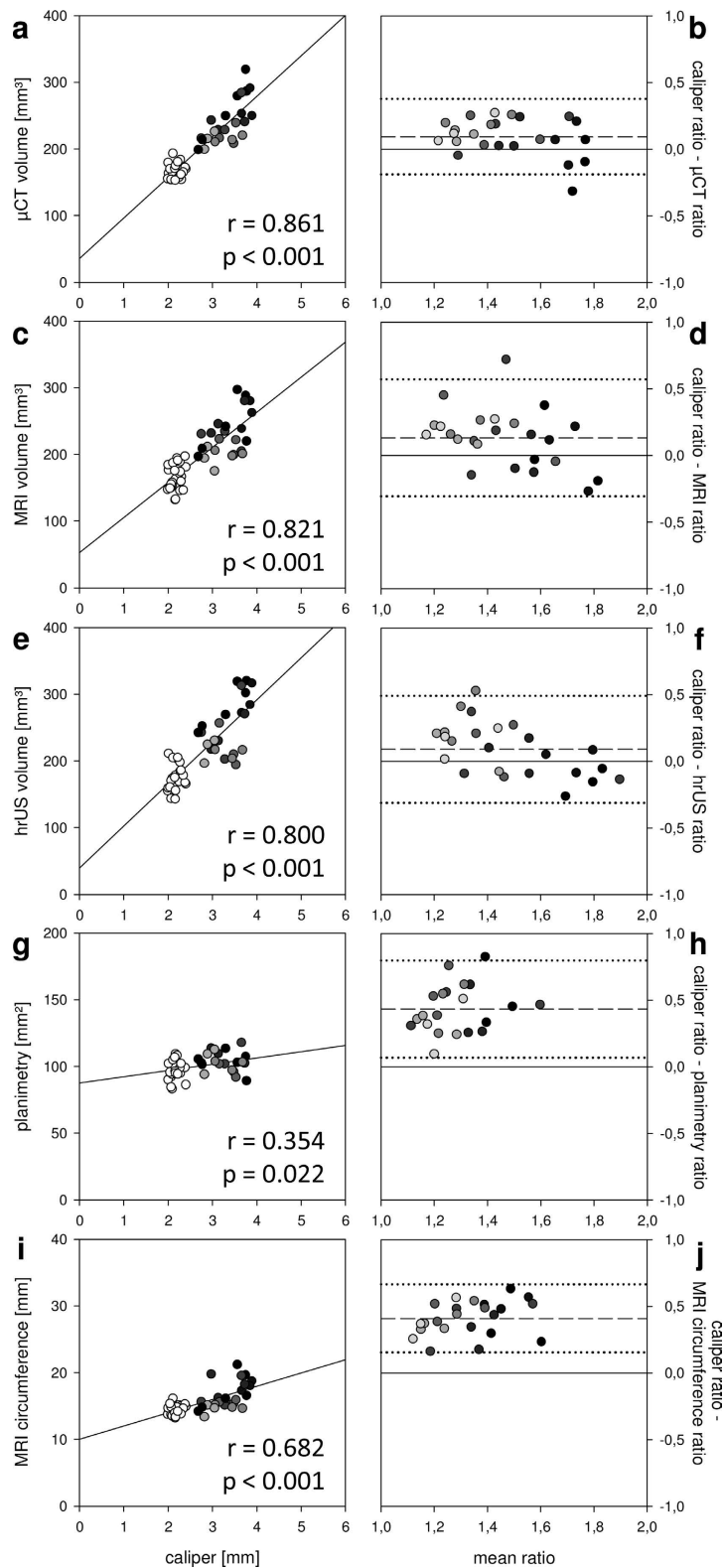


Figure 7. Caliper-measured paw thickness versus other hindlimb volumetry modalities. (a–j) Linear correlations (a,c,e,g,i) and Bland-Altman plots (b,d,f,h,j) comparing caliper-measured paw thickness with other hindlimb volumetry modalities. The caliper correlated well with 3D volumetry (a–f) but no or low correlation with planimetry (g,h) and circumferential length (i,j) was recorded. Importantly, hindlimb ratios based on paw thickness were higher than those calculated with the other modalities (n = 48 for μ CT, MRI, hrUS, MRI circumference and caliper; n = 42 for planimetry; day 3–10 = black to bright grey circles; non-operated control limbs = white circles; dashed line = mean difference between ratios; dotted line = double standard deviation).

Animal model. Mice were anesthetized by intraperitoneal injection of ketamine (75 mg/kg body weight; Ursotamin, Serumwerk Bernburg AG, Bernburg, Germany) and xylazine (15 mg/kg body weight; Rompun, Bayer, Leverkusen, Germany). To induce lymphedema, we combined and modified the surgical steps of previously established hindlimb models^{19,38}. For this purpose, hindlimbs were depilated (Nair hair removal cream, Church & Dwight Canada Corp., Mississauga, ON, Canada) and the animals were placed in prone position. After intradermal injection of 15 μ L methylene blue 10% (Carl Roth GmbH, Karlsruhe, Germany) in the right middle phalanx with a 31 Gauge syringe (Hamilton Bonaduz AG, Bonaduz, Switzerland) (Fig. 1a), a circular incision was performed over the popliteal fossa. The stained afferent lymphatic vessels were ligated with 10/0 monofilament (Monosof; Covidien Deutschland GmbH, Neustadt/Donau, Germany) and the fat pad containing the popliteal lymph node and the efferent lymphatic vessels was microsurgically resected under continuous hemostasis (Erbe Kauter B; Erbe Elektromedizin GmbH, Tübingen, Germany) maintaining the surrounding muscles intact (Fig. 1b,c). Finally, circumferential epifascial cautery was performed to block superficial lymphatic vessels. The skin was closed with interrupted 5/0 monofilament (Prolene; Ethicon, Johnson & Johnson Medical GmbH, Norderstedt, Germany). Postoperative analgesia was provided for 3 days with tramalhydrochloride (40 mg/100 mL drinking water; Grünenthal GmbH, Aachen, Germany). The contralateral hindlimb was not operated and served as internal control.

μ CT. Imaging was performed in isoflurane anesthesia and supine position by means of the *in vivo* SkyScan 1076 μ CT system (Bruker, Kontich, Belgium). The 35 mm transaxial field of view (FOV) allowed imaging of both hindlimbs. An oversize scan, which was performed by connecting 3 scans with an estimated acquisition time of 11 min, enabled the visualization of the hindlimbs from phalanx to pelvis. The scan parameters were 35 μ m pixel size, 50 kV, 200 μ A, 0.5 mm Al filter, angular rotation step 0.8° and an exposure time of 58 ms. The recorded images were segmented using an adaptive thresholding algorithm provided by the SkyScan software CTan, because the observation of bone and soft tissue precluded the use of global thresholding⁴⁶. Quantitative analysis of the 3D measurements was performed by means of the appropriate software licensed to Bruker (CTan).

MRI. MRI was performed in isoflurane anesthesia using a linear polarized coil (inner diameter: 38 mm) developed for imaging of the mouse abdomen and a horizontal bore 9.4 T MRI animal scanner equipped with the operating software Paravision 6.0.1 (Bruker Biospin Inc., Billerica, MA, USA) (Fig. S1f). Because hindlimb imaging was prone to partial volume effects, we used a water-filled phantom to facilitate sufficient magnetic field homogeneity.

The hindlimb protocol consisted of a fast low angle shot based 3D localizer, followed by extensive 1st and 2nd order shimming of the entire FOV. Subsequently, adjustments of resonance frequency, radio frequency pulse strength and receiver gain were performed and slice geometry was adjusted to animal placement within the isocenter. 3D volumetry datasets were recorded with a 3D rapid acquisition relaxation enhanced (RARE) sequence with flipback RF pulse, facilitating T2-weighted imaging with low repetition time (TR). Datasets were recorded with the following settings: Slice orientation coronal, TR 500 ms, echo time 33 ms, RARE factor 16, excitation/re-focussing flip angle 90°/180°, number of averages 2, zero fill in read phase and slice directions 2, FOV 42 \times 35 \times 20 mm³, matrix size 420 \times 350 \times 200, resulting voxel size 100 \times 100 \times 100 μ m³. Axial MR images were reconstructed with the MRI scanner operating software and exported as DICOM (Digital Imaging and Communications in Medicine) images for further processing with the free DICOM software OsiriX™ Lite (version v7.0.3; Pixmeo, Geneva, Switzerland). The hindlimb volumes were manually calculated by integrating the outlined areas for MRI measurements using a spreadsheet program (Office Excel® 2007; Microsoft, Redmond, WA, USA).

hrUS. Mice were anesthetized with isoflurane and put on a heated stage (Fig. S1g). Chemical depilation (Nair hair removal cream) was done to prevent air trapped in the fur from interfering with ultrasound coupling into the animal. To distinguish between the stage and the hindlimb, ultrasound coupling gel (Aquasonic 100, Parker, Fairfield, NJ, USA) was circumferentially applied to hindlimbs and pelvis (Fig. S1g).

Imaging was performed by means of a Vevo 770 high-resolution ultrasound system (VisualSonics, Toronto, ON, Canada) and a real-time microvisualization 707B Scanhead (VisualSonics) with a center frequency of 30 MHz and a focal depth of 12.5 mm. For 3D imaging the scanhead, driven by a linear motor, scanned first the non-operated and then the operated hindlimb. The technique yielded two-dimensional (2D) images at parallel and uniformly spaced 100 μ m steps. The 2D image planes enabled rapid 3D image reconstruction, displaying a dynamic cube view format, as previously described⁴⁷. Volume calculations were performed with the software licensed VisualSonics (Vevo 770 V2.3.0).

Histology and immunohistochemistry. For light microscopy, formalin-fixed paws were embedded in paraffin. The paraffin blocks were cut until the desired plane and decalcified with Osteomoll® (Merck KGaA, Darmstadt, Germany) for 10 min. Subsequently, 2 μ m sections were cut and stained with hematoxylin and eosin (HE) according to standard procedures. For the immunohistochemical detection of lymphatic vessels, additional sections were stained with a polyclonal rabbit IgG-antibody against lymphatic vessel endothelial hyaluronan receptor (LYVE)-1 (1:50; Abcam, Cambridge, UK). A peroxidase-labeled goat-anti-rabbit IgG-antibody (1:200; Dianova, Hamburg, Germany) served as secondary antibody and 3-amino-9-ethylcarbazole (ready-to-use, ab64252; Abcam) was added as chromophor. The sections were counterstained with Mayer's hemalum solution (HX948000; Merck, Darmstadt, Germany) and examined under a BX60 microscope (Olympus, Hamburg, Germany) for qualitative analyses.

Statistics. Data were analyzed for normal distribution and equal variance. Differences between non-operated and operated legs were tested by an unpaired Student's t test. Linear correlation (Pearson's coefficient of

correlation for parametric distribution or Spearman's coefficient of correlation for nonparametric distribution) and Bland-Altman analyses were performed to evaluate correspondence of different measurement techniques detecting hindlimb swelling. To create a Bland-Altman plot, the mean of all measured values detected by two different observers or techniques was plotted on the horizontal axis and the difference between the two types of measurement was plotted on the vertical axis⁴⁸. Values were expressed as mean \pm standard error of the mean (SEM). Statistical significance was set for $p < 0.05$.

References

- Cueni, L. N. & Detmar, M. The lymphatic system in health and disease. *Lymphat. Res. Biol.* **6**, 109–122 (2008).
- Rockson, S. G. Current concepts and future directions in the diagnosis and management of lymphatic vascular disease. *Vasc. Med.* **15**, 223–231 (2010).
- Szuba, A. & Rockson, S. G. Lymphedema: anatomy, physiology and pathogenesis. *Vasc. Med.* **2**, 321–326 (1997).
- Alitalo, K. The lymphatic vasculature in disease. *Nat. Med.* **17**, 1371–1380 (2011).
- Mortimer, P. S. & Rockson, S. G. New developments in clinical aspects of lymphatic disease. *J. Clin. Invest.* **124**, 915–921 (2014).
- Karkkainen, M. J. *et al.* Missense mutations interfere with VEGFR-3 signalling in primary lymphoedema. *Nat. Genet.* **25**, 153–159 (2000).
- Bramos, A. *et al.* Prevention of Postsurgical Lymphedema by 9-cis Retinoic Acid. *Ann. Surg.* **264**, 353–361 (2016).
- Avraham, T. *et al.* Fibrosis is a key inhibitor of lymphatic regeneration. *Plast. Reconstr. Surg.* **124**, 438–450 (2009).
- Hadamitzky, C. & Pabst, R. Acquired lymphedema: an urgent need for adequate animal models. *Cancer Res.* **68**, 343–345 (2008).
- DiSipio, T., Rye, S., Newman, B. & Hayes, S. Incidence of unilateral arm lymphoedema after breast cancer: a systematic review and meta-analysis. *Lancet Oncol.* **14**, 500–515 (2013).
- Frueh, F. S. *et al.* Animal models in surgical lymphedema research—a systematic review. *J. Surg. Res.* **200**, 208–220 (2016).
- Mendez, U., Brown, E. M., Ongstad, E. L., Slis, J. R. & Goldman, J. Functional recovery of fluid drainage precedes lymphangiogenesis in acute murine foreleg lymphedema. *Am. J. Physiol. Heart. Circ. Physiol.* **302**, H2250–H2256 (2012).
- Mendez, U., Stroup, E. M., Lynch, L. L., Waller, A. B. & Goldman, J. A chronic and latent lymphatic insufficiency follows recovery from acute lymphedema in the rat foreleg. *Am. J. Physiol. Heart. Circ. Physiol.* **303**, H1107–H1113 (2012).
- Tammela, T. *et al.* Therapeutic differentiation and maturation of lymphatic vessels after lymph node dissection and transplantation. *Nat. Med.* **13**, 1458–1466 (2007).
- Aschen, S. Z. *et al.* Lymph node transplantation results in spontaneous lymphatic reconnection and restoration of lymphatic flow. *Plast. Reconstr. Surg.* **133**, 301–310 (2014).
- Cheng, M. H. *et al.* The mechanism of vascularized lymph node transfer for lymphedema: natural lymphaticovenous drainage. *Plast. Reconstr. Surg.* **133**, 192e–198e (2014).
- Joseph, W. J. *et al.* Sterile inflammation after lymph node transfer improves lymphatic function and regeneration. *Plast. Reconstr. Surg.* **134**, 60–68 (2014).
- Nguyen, D. H. *et al.* Quantity of lymph nodes correlates with improvement in lymphatic drainage in treatment of hind limb lymphedema with lymph node flap transfer in rats. *Microsurgery.* **36**, 239–245 (2016).
- Hwang, J. H. *et al.* Therapeutic lymphangiogenesis using stem cell and VEGF-C hydrogel. *Biomaterials.* **32**, 4415–4423 (2011).
- Yoshida, S. *et al.* Adipose-derived stem cell transplantation for therapeutic lymphangiogenesis in a mouse secondary lymphedema model. *Regen. Med.* **10**, 549–562 (2015).
- Sommer, T. *et al.* Quantification of lymphedema in a rat model by 3D-active contour segmentation by magnetic resonance imaging. *Lymphat. Res. Biol.* **10**, 25–29 (2012).
- Yang, C. Y. *et al.* Developing a Lower Limb Lymphedema Animal Model with Combined Lymphadenectomy and Low-dose Radiation. *Plast. Reconstr. Surg. Glob. Open.* **2**, e121 (2014).
- Schneider, C. A., Rasband, W. S. & Eliceiri, K. W. NIH Image to ImageJ: 25 years of image analysis. *Nat. Methods.* **9**, 671–675 (2012).
- Baumeister, R. G. *et al.* Microsurgical Lymphatic Vessel Transplantation. *J. Reconstr. Microsurg.* **32**, 34–41 (2016).
- Koshima, I., Inagawa, K., Urushibara, K. & Moriguchi, T. Supermicrosurgical lymphaticovenular anastomosis for the treatment of lymphedema in the upper extremities. *J. Reconstr. Microsurg.* **16**, 437–442 (2000).
- Becker, C., Assouad, J., Riquet, M. & Hidden, G. Postmastectomy lymphedema: long-term results following microsurgical lymph node transplantation. *Ann. Surg.* **243**, 313–315 (2006).
- Lähteenhuo, M. *et al.* Growth factor therapy and autologous lymph node transfer in lymphedema. *Circulation.* **123**, 613–620 (2011).
- Honkonen, K. M. *et al.* Lymph node transfer and perinodal lymphatic growth factor treatment for lymphedema. *Ann. Surg.* **257**, 961–967 (2013).
- Hwang, J. H., Lee, C. H., Lee, H. H. & Kim, S. Y. A new soft tissue volume measurement strategy using ultrasonography. *Lymphat. Res. Biol.* **12**, 89–94 (2014).
- Sevick-Muraca, E. M., Kwon, S. & Rasmussen, J. C. Emerging lymphatic imaging technologies for mouse and man. *J. Clin. Invest.* **124**, 905–914 (2014).
- Kobayashi, H. *et al.* Comparison of dendrimer-based macromolecular contrast agents for dynamic micro-magnetic resonance lymphangiography. *Magn. Reson. Med.* **50**, 758–766 (2003).
- Pan, D., Suzuki, Y., Yang, P. C. & Rockson, S. G. Indirect magnetic resonance lymphangiography to assess lymphatic function in experimental murine lymphedema. *Lymphat. Res. Biol.* **4**, 211–216 (2006).
- Mounzer, R. *et al.* Dynamic imaging of lymphatic vessels and lymph nodes using a bimodal nanoparticulate contrast agent. *Lymphat. Res. Biol.* **5**, 151–158 (2007).
- Hayashi, K., Nakamura, M. & Ishimura, K. Near-infrared fluorescent silica-coated gold nanoparticle clusters for x-ray computed tomography/optical dual modal imaging of the lymphatic system. *Adv. Healthc. Mater.* **2**, 756–763 (2013).
- Martel, C. *et al.* Photoacoustic lymphatic imaging with high spatial-temporal resolution. *J. Biomed. Opt.* **19**, 116009 (2014).
- Shejawal, N., Menon, S. & Shailajan, S. A simple, sensitive and accurate method for rat paw volume measurement and its expediency in preclinical animal studies. *Hum. Exp. Toxicol.* **33**, 123–129 (2014).
- Lee-Donaldson, L. *et al.* Refinement of a rodent model of peripheral lymphedema. *Lymphology.* **32**, 111–117 (1999).
- Oashi, K. *et al.* A new model of acquired lymphedema in the mouse hind limb: a preliminary report. *Ann. Plast. Surg.* **69**, 565–568 (2012).
- Park, H. S. *et al.* Modification of a rodent hindlimb model of secondary lymphedema: surgical radicality versus radiotherapeutic ablation. *Biomed. Res. Int.* **2013**, 208912 (2013).
- Damstra, R. J., Glazenburg, E. J. & Hop, W. C. Validation of the inverse water volumetry method: A new gold standard for arm volume measurements. *Breast Cancer Res. Treat.* **99**, 267–273 (2006).
- Pan, D., Han, J., Wilburn, P. & Rockson, S. G. Validation of a new technique for the quantitation of edema in the experimental setting. *Lymphat. Res. Biol.* **4**, 153–158 (2006).
- Shioya, R. *et al.* Prevention of Lymphedematous Change in the Mouse Hindlimb by Nonvascularized Lymph Node Transplantation. *Ann. Plast. Surg.* **76**, 442–445 (2016).

43. Fajardo, K. A. *et al.* Bilateral lower extremity inflammatory lymphedema in Air Force basic trainees: clinical and epidemiologic study of a new disease entity. *JAMA Dermatol.* **151**, 395–400 (2015).
44. Zhou, H. F., Chan, H. W., Wickline, S. A., Lanza, G. M. & Pham, C. T. Alphavbeta3-targeted nanotherapy suppresses inflammatory arthritis in mice. *FASEB J.* **23**, 2978–2985 (2009).
45. Xin, W. *et al.* Methyl salicylate lactoside inhibits inflammatory response of fibroblast-like synoviocytes and joint destruction in collagen-induced arthritis in mice. *Br. J. Pharmacol.* **171**, 3526–3538 (2014).
46. Laperre, K. *et al.* Development of micro-CT protocols for *in vivo* follow-up of mouse bone architecture without major radiation side effects. *Bone.* **49**, 613–622 (2011).
47. Fenster, A., Downey, D. B. & Cardinal, H. N. Three-dimensional ultrasound imaging. *Phys. Med. Biol.* **46**, R67–R99 (2001).
48. Bland, J. M. & Altman, D. G. Statistical methods for assessing agreement between two methods of clinical measurement. *Lancet.* **1**, 307–310 (1986).

Acknowledgements

We are grateful for the excellent assistance of Janine Becker and Ruth Nickels. Special thanks go to Carol De Simio (University Hospital Zurich) for drawing Figure 5a. FS Frueh received support from the German Society for Lymphology (DGL; grant number Fo0315), the Swiss Society for Lymphology (SGL) and S&T AG Microsurgical Instruments (Neuhausen, Switzerland).

Author Contributions

F.S.F., C.K. and L.G. designed the study; performed surgery, volumetric measurements, data analysis and wrote the manuscript. A.M. performed MR volumetry and wrote the manuscript. E.G. helped with animal model establishment; critical manuscript revision. N.L. and P.G. critical manuscript revision. M.D.M. and M.W.L. designed the study, analyzed data and critically revised the manuscript. All authors reviewed and approved the final version of the manuscript.

Additional Information

Supplementary information accompanies this paper at <http://www.nature.com/srep>

Competing financial interests: The authors declare no competing financial interests.

How to cite this article: Frueh, F. S. *et al.* High-resolution 3D volumetry versus conventional measuring techniques for the assessment of experimental lymphedema in the mouse hindlimb. *Sci. Rep.* **6**, 34673; doi: 10.1038/srep34673 (2016).



This work is licensed under a Creative Commons Attribution 4.0 International License. The images or other third party material in this article are included in the article's Creative Commons license, unless indicated otherwise in the credit line; if the material is not included under the Creative Commons license, users will need to obtain permission from the license holder to reproduce the material. To view a copy of this license, visit <http://creativecommons.org/licenses/by/4.0/>

© The Author(s) 2016